Atom scattering from isolated adsorbates on surfaces: Rainbows, diffraction interferences, and trapping resonances

A. T. Yinnon, R. Kosloff, and R. B. Gerber
Department of Physical Chemistry and The Fritz Haber Research Center for Molecular Dynamics, The Hebrew University of Jerusalem, Jerusalem 91904, Israel

(Received 19 January 1988; accepted 23 February 1988)

The scattering of He atoms from a CO molecule adsorbed on a Pt surface is studied theoretically by methods that include: (1) Numerically exact solutions of the time-dependent Schrödinger equation for the scattered wave packet; (2) The sudden approximation; (3) Classical trajectories. The methods are used to obtain detailed insight into the collision dynamics, and to predict and understand interesting features in the angular intensity distribution of the scattered atoms. The analysis and interpretation of the exact quantum results is facilitated by calculations of the probability current density of the scattered particles. Some of the main results are: (i) The angular intensity distribution exhibits nonspecular maxima of two types: Several of the peaks are rainbow effects induced by the adsorbate, while others (at angles nearer to the specular) are Fraunhofer diffraction interferences. Both types of peaks contain useful, largely complementary, information on adsorbate geometry and on the He/adsorbate interaction. (ii) The angular intensity distribution is quantitatively sensitive to the adsorbate distance from the surface, suggesting possible determination of that distance from experimental data. (iii) The corrugation due to the adsorbate leads to scattering resonances associated with temporary trapping of the scattered atom at the defect site. This is a new effect of potential importance for experimental studies of atom/defect interactions. The results obtained here suggest that He scattering from isolated adsorbates exhibits distinct, substantial effects, measurement of which should yield very useful data on the adsorbates and on their interactions with gas-phase atoms.

I. INTRODUCTION

Isolated defects on crystalline surfaces, such as steps, adsorbates, and vacancies, often greatly affect the physical and chemical behavior of the surfaces. Determination of the structure and of other microscopic properties of such defects, of which little is known at the present time, is thus a major goal of surface science. Results in the last few years indicate that He scattering is potentially a very powerful probe of surface defects and their properties.[1] The first, and very major, experimental direction in this subject focused on the attenuation of the specular scattering from the surface due to the presence of the defects.[1–5] In particular, Comsa and co-workers[1,3–5] were able to extract a wealth of information on surface defects and their mutual attractions from measurements of the attenuation of the specular scattering as defect concentration is varied. Also, there have been several theoretical studies and calculations of the cross section for scattering by a defect, a concept directly related to the attenuation of the specular scattering.[6–9] A second important line in studying surface imperfections by He scattering has been the investigation of the angular intensity distribution. Theoretical studies by the present authors[10] and independently by Heuer and Rice[11] predicted the occurrence of weak maxima in the nonspecular intensity distribution for atom scattering from isolated adsorbates on smooth or periodic surfaces. Gerber *et al.*[10(a)] and Yinnon *et al.*[10(b)] found that the nonspecular maxima of the angular distribution in their calculations were rainbow effects due to the local corrugation caused by the defect. In a recent study[12] Lahee *et al.* reported observation of undulations in the angular intensity distribution of He atoms scattered from isolated CO molecules on a Pt(111) surface. This was interpreted by the authors as Fraunhofer interference oscillations.[13] Although both experimentally and theoretically the subject is in a very early stage of development, the abovementioned progress is encouraging. As the available theoretical calculations suggest,[10,12,14] angular intensity distributions for scattering from a defect can, in principle, furnish very useful information on the geometry of the imperfection, and on the interactions between the latter and the He atom.

The present article explores the collision dynamics of an incoming He atom with an isolated CO molecule adsorbed on flat Pt surfaces with two purposes in mind. First, interesting new effects in the scattering induced by the adsorbate are demonstrated. Perhaps the main such effects are scattering resonances corresponding to trapping of the He atom by the impurity. Second, we seek to clarify the relation between rainbows and Fraunhofer peaks in the angular intensity distribution, and to show that the two features are distinct, but can both be found in the same intensity distribution under certain conditions. We discuss the information contained in each of the two features.

The structure of the article is as follows: In Sec. II we discuss the model used for the adsorbate and for its interaction with the He atom. Section III briefly describes the meth-

 0021-9606/88/117209-12$02.10

ods employed for studying the collision dynamics and the scattering intensities. Section IV gives an analysis of the results. Concluding remarks are brought in Sec. V.

II. THE MODEL SYSTEM

The present study deals with the scattering of a He atom from an isolated CO molecule chemisorbed upon a smooth Pt surface. The molecule and the underlying surface will be treated as a static, nonvibrating target. Obviously, vibrations of the adsorbate and of the surface are expected to affect quantitatively the collision dynamics and the angular intensity distribution measured in molecular beam experiments. However, results of calculations using a rigid, nonvibrating surface system should be useful at least for studying the main qualitative effects. Moreover, for diffraction scattering from crystalline surfaces, the effect of surface vibrations on the scattering intensities can be represented approximately by a simple Debye–Waller factor.[14] A similar description may be successful also for the angular intensity distribution in scattering from surface defects.

The Pt surface will be treated in most of the calculations reported here as completely flat. For a very low corrugation surface such as Pt(111), this should be a good approximation.

In the work reported here, scattering calculations were carried out for three models of the interaction potential between He and the [adsorbate + Pt surface]:

A. Gas-phase He/CO interaction

This model takes the He/[CO + Pt] potential function to be of the form

$$V(x,y,z) = V_s(z) + V_{AD}(x,y,z)\,, \tag{1}$$

where $V_s(z)$ represents the interaction between He and a Pt(111) surface, assumed completely smooth, and V_{AD} is the interaction potential between He and CO in the gas phase. The coordinate z measures the distance of the He atom from the surface plane, while (x,y) are the coordinates in parallel to the surface plane. For the gas-phase He/CO interaction we took an isotropic potential determined from the experiments of Butz *et al.*[15] This potential depends only on the distance R between He and the center of mass of the CO: $V_{AD}(x,y,z) = V_{AD}(\mathbf{r} - \mathbf{r}_{AD}) = V_{AD}(R)$, where $\mathbf{r}$ is the position vector of the He, and $\mathbf{r}_{AD}$ the position vector of the CO c.m. The gas-phase He/CO potential of Butz *et al.*[15] has a well depth of $\epsilon = 2.37$ meV, and a minimum distance of $R_m = 3.5$ A. For the He/Pt interaction a Morse potential was used

$$V_s(z) = D_s\left[e^{-2\alpha(z-z_m)} - 2e^{-\alpha(z-z_m)}\right]. \tag{2}$$

The steepness parameter of the Morse potential was taken to have the value of $\alpha = 0.6$ bohr^{-1}, typical of He interactions with metal surfaces. The value of $D_s = 4.0$ meV, given by Harris *et al.*[16] was employed. The value of z_m was adjusted to yield a specified distance of the CO c.m. (the position of which was defined as $z = 0$) from the surface plane of Pt, leading to $z_m = 2.3$ bohr. The interaction potential (1) is definitely not quantitatively correct. Indeed, the experimental cross sections for He scattering from CO on Pt(111) as a function of incident energy and angle are not satisfactorily reproduced by this potential.[9] Nevertheless, we expect this potential to be realistic on a semiquantitative footing. This should suffice for our purpose of searching for qualitative effects in the angular intensity distribution. However, in order to assess the sensitivity of the results to the potential used, calculations were carried out also for other model potentials.

B. The potential of Jonsson *et al.*[6]

This potential has the form of Eq. (1). However, $V_{AD}(\mathbf{r} - \mathbf{r}_{AD}) = V_{AD}(R)$ was not taken in this case as the gas-phase He/CO interaction. Rather, we employ the Lennard-Jones potential $V_{AD}(R)$ obtained by Jonsson *et al.* by the fitting of the energy-dependence of the measured cross section for He/[CO + Pt(111)].[6] This potential has a well-depth of $\epsilon = 1.38$ meV, and a minimum distance $R_m = 4.3$ A, and it differs therefore considerably from the gas-phase potential discussed above. Also the potential of Jonsson *et al.*, as all currently available potential functions for He/[CO + Pt(111)], must not be regarded as quantitatively true since, e.g., it fails to reproduce the experimental variation of the measured cross section with the incidence angle.[9]

C. The potential of Liu and Gumhalter[17]

This potential function, again of the general form of Eq. (1), introduces an atom/adsorbate interaction that is corrected for surface polarization effects. $V_{AD}(\mathbf{r} - \mathbf{r}_{AD})$ is given in this model by

$$V_{AD}(\mathbf{r} - \mathbf{r}_{AD}) = V_{AD}^{(d)}(\mathbf{r} - \mathbf{r}_{AD}) + V_{AD}^{(im)}(\mathbf{r} - \mathbf{r}_{AD}) + V_{AD}^{(int)}(\mathbf{r} - \mathbf{r}_{AD})\,, \tag{3}$$

where $V_{AD}^{(d)}$ is the direct, gas-phase-like interaction between the atom and the adsorbed molecule. For the repulsive part of this interaction, Liu and Gumhalter employed the exponential potential given by Gordon and McGinnis for gas-phase He/CO.[18] The attractive, long-range part of $V_{AD}^{(d)}$ as employed by Gumhalter and Liu is given by

$$V_{AD}^{(d)}(\mathbf{r} - \mathbf{r}_{AD}) = -C_{ab}\frac{(2+4\mu)}{R^6} \times\left[1 - \frac{1-\mu}{1+2\mu}P_2(\cos\theta)\right], \tag{4}$$

where $R = |\mathbf{r} - \mathbf{r}_{AD}|$, θ is the angle between $\mathbf{R} = \mathbf{r} - \mathbf{r}_{AD}$ and the normal to the surface. μ is the ratio of transverse and longitudinal adsorbate polarizabilities. $V_{AD}^{(im)}$ in Eq. (3) represents the interaction of the He with the adsorbate image in the surface plane. $V_{AD}^{(int)}$ is an interference term between the interaction of the atom with the adsorbate, and its interaction with the pure image. The functional forms of these interactions, and the parameters for He/[CO + Pt] are given in Ref. (17) and Ref. (9). As the calculations show, the surface mediated interaction terms have little effect on the angular intensity distribution studied here. On the other hand, the adsorbate location with respect to the surface plane (given by $\mathbf{r}_{AD}$) was found to be of crucial importance. We varied

this geometric parameter in the calculations, to demonstrate its effect on the observable angular intensity distribution.

D. Potential for corrugated surfaces

We carried out several calculations to assess the effect of the corrugation of the underlying crystalline surface on the scattering from the adsorbate. This topic was already very briefly examined by Gerber *et al.*[10] The potential function employed in this case is also of the additive form (1), but the He/crystal interaction component V_s is taken as

$$V_s(z,x,y) = D_s\left[e^{-2\alpha(z-z_m)} - 2e^{-\alpha(z-z_m)}\right] + \beta D_s e^{-2\alpha(z-z_m)} \times\left[\cos\left(\frac{2\pi}{a}x\right) + \cos\left(\frac{2\pi}{a}y\right)\right] \quad (5)$$

which is the familiar Lennard-Jones–Devonshire model.[19] Here a is the lattice constant of the surface, and β is the corrugation parameter. In the calculations we used the value of $\beta = 0.1$ [which is certainly unrealistically high for Pt(111) and other smooth metal surfaces] in order to obtain strong, noticeable effects. Such a corrugation is roughly in the correct range for alkali halide surfaces such as LiF(001). For the He adsorbate interaction term we used in this case the gas-phase He/CO potential.

III. THE METHODS

Several methods were used in this study in order to compute the angular intensity distribution of the scattered atoms and to gain insight into the ways in which the collision dynamics is reflected in that distribution. The methods employed were: (1) The solution of the time-dependent Schrödinger equation for the scattering process by the FFT algorithm[20–22]; (2) The sudden approximation[23–26]; (3) Classical trajectory calculations. Since these methods were already discussed extensively in previous articles, only brief comments will be made.

To obtain the time evolution of the wave packet which describes the scattering process, the FFT method numerically solves the time-dependent Schrödinger equation

$$i\frac{\partial\Psi(\mathbf{r},t)}{\partial t} = \left(-\frac{\hbar^2}{2m}\nabla_r^2 + V(\mathbf{r})\right)\Psi(\mathbf{r},t)\,, \quad (6)$$

where $\mathbf{r}$ is the position vector of the scattered atom and m its mass. The technique, due to Kosloff and Kosloff[20] uses the fast Fourier transform algorithm (FFT) to evaluate the action of the kinetic energy operator in Eq. (6) upon the wave function at each time point. The propagation in time of the wave function was obtained in the present study by expanding the evolution operator e^{-iHt} by a Chebychev polynomial series which is discussed elsewhere,[21,22] and is a very efficient algorithm. To facilitate the physical interpretation of the effects found in terms of the computed wave packets, we made use here of the probability current density, a vector quantity defined by [27]:

$$\mathbf{j}(\mathbf{r},t) = \mathrm{Re}\left[\Psi^*\frac{\hbar}{im}\nabla\Psi\right]. \quad (7)$$

As will be seen later, analysis of this quantity offers insights into the formation mechanism of resonances, interference structures, etc.

Both quantum-mechanical[9,10,22,25] and semiclassical[13,22,28] wave packet methods have previously been applied to the study of scattering from defects, and their advantages for this purpose are apparent. For example, the time-independent close coupling technique, extensively in use for scattering from crystalline surfaces, requires expansion of the scattering wave function in a discrete basis (for which the diffraction states are employed in the case of a periodic lattice). No such basis is available in the case of a surface with defects, when the allowed final momentum states form a continuum.[14,22] The wave packet methods do not require a basis set expansion, and are thus applicable to the present problem.[22]

Another very useful tool in studies of atom scattering from defects has been the sudden approximation,[23–26,9] which has the advantage of offering an explicit expression for the angular intensity distribution, but is restricted to certain systems and scattering conditions. Basically, the sudden approximation requires that the momentum transfer in the direction parallel to the surface be small compared with the momentum transfer normal to the surface, i.e.,[9,23,24]

$$|\mathbf{K}' - \mathbf{K}| \ll 2k_z\,, \quad (8)$$

where k_z is the incident wave number in the z direction; $\mathbf{K}$ is the incident wave vector in parallel to the surface plane, and $\mathbf{K}'$ is any intermediate or final wave vector in parallel to the surface plane which plays a significant role in the scattering process. For a surface of area A which contains a single defect, the angular intensity distribution is given by the function

$$P_{\mathbf{K}\to\mathbf{K}'} = \frac{1}{A^2}\left|\int e^{i(\mathbf{K}'-\mathbf{K})\cdot\rho}e^{2i\eta(\rho)}d\rho\right|^2, \quad (9)$$

where $\rho = (x,y)$, and $\eta(\rho)$ is the scattering phase shift computed for fixed ρ, given by

$$\eta(\rho) = \int_{z_0}^{\infty} dz\left\{\left[k_z^2 - 2mV(x,y,z)/\hbar^2\right]^{1/2} - k_z\right\} - k_z z_0\,, \quad (10)$$

where z_0 is the classical turning point pertaining to the integrand in Eq. (10). Condition (8) for the validity of the sudden approximation is expected to break down for systems of high corrugation, and an isolated adsorbate on an otherwise flat surface generally represents, for realistic parameters, a very substantial local corrugation.[24,25] Nevertheless, previous calculations have shown that the sudden approximation reproduces rather well many features of the scattering from isolated adsorbates.[25] Features for which it breaks down are, e.g., intensity peaks due to double collision events (in which the incoming atom first hits the surface and then the adsorbate or *vice versa*), which are a particularly sensitive manifestation of strong corrugation. The sudden approximation is thus useful for the interpretation of these features for which it works, and offers useful insights also at the points where it breaks down.

Another tool employed in this study for gaining understanding of the collision dynamics are classical trajectory calculations. To obtain an angular intensity distribution

from such trajectory calculations we must employ a sufficiently dense sample set of initial (x,y) values for the incoming atom so as to adequately represent all collisions between the beam particles and the surface segment that contains the defect. Typically, about 2000 trajectories were used in each such calculation. Quantum effects, in particular interferences, are important in such collisions, hence classical trajectory results for the angular intensity distribution are bound to be seriously flawed. Nevertheless, individual trajectories do offer important and valid insight into many qualitative aspects of the collision dynamics.

IV. RESULTS AND DISCUSSION

The results will be outlined by examining separately each of several properties or features of the angular intensity distribution.

A. Single- and double-collision rainbows and Fraunhofer diffraction

Figure 1 shows the results of calculations within the sudden approximation of He scattered from Pt(111), using the fitted potential of Jonsson *et al.*,[6] discussed in Sec. II. For simplicity, a one dimensional "surface" is used, i.e., the interaction potential and the collision dynamics, were restricted to the (z,x) plane only, and the y coordinate was not included. A normal incidence collision was treated with collision wave number $k_z = 2.47\ \text{bohr}^{-1}$. The angular intensity in Fig. 1 exhibits, in addition to the large specular peak, also six additional peaks, the pattern being obviously symmetrical in the momentum transfer $\Delta K_x = K_x' - K_x (K_x = 0)$ in the x direction. It is useful to employ a stationary-phase, approximate evaluation of the sudden scattering amplitude, as in Ref. 25. The crude quasiclassical stationary-phase limit of Eq. (9) predicts a rainbow whenever[25]

$$\frac{\partial^2 \eta}{\partial x^2} = 0 . \tag{11}$$

In the classical limit, this should show up as a singularity in the angular intensity distribution at momentum transfer ΔK_x such that

$$\Delta K_x = -2 \frac{\partial \eta(x)}{\partial x} , \tag{12}$$

where x is the stationary-phase point of the integrand (9) for momentum transfer ΔK_x. The singularity of the crude classical evaluation is smoothed into a finite peak in more refined calculations. Using the phase-shift $\eta(x)$ calculated from the potential of Jonsson *et al.*,[6] we find that rainbows are predicted for $\Delta K_x = \pm 1.26\ \text{bohr}^{-1}$, in good agreement with the peaks at $\Delta K_x \sim 1.3\ \text{bohr}^{-1}$ in Fig. 1. We therefore identify this symmetrical pair of peaks as rainbows. We did not find a point x that satisfies the rainbow condition (11), i.e., inflection points of the phase shift, for the maxima at $\Delta K_x = \pm 0.48\ \text{bohr}^{-1}$, $\Delta K_x = \pm 2.20\ \text{bohr}^{-1}$. We shall see below that the peaks at $\Delta K_x = \pm 0.48\ \text{bohr}^{-1}$ are Fraunhofer diffraction effects. Rainbows in atom scattering from defects were found and analyzed in Refs. 10 and 25 and the sudden approximation was useful in identifying some of the rainbows in these calculations.

We consider now Fig. 2, the results of numerically exact wave packet calculations for the same potential and scattering conditions as shown in Fig. 1. Although the maxima at $\Delta K_x = 1.56\ \text{bohr}^{-1}$ are shifted from the rainbow positions in the sudden intensities of Fig. 1, the shift is not very large, and it seems reasonable to identify these peaks as the "exact" manifestations of the rainbows found in the sudden approximation. For the peaks at $\Delta K_x = \pm 0.48\ \text{bohr}^{-1}$, $\Delta K_x = \pm 0.85\ \text{bohr}^{-1}$, $\Delta K_x = \pm 1.22\ \text{bohr}^{-1}$, we suggest that these can be interpreted as Fraunhofer interference maxima. Indeed, Lahee *et al.*[12] semiquantitatively interpreted their experimental results on He scattering from CO on Pt(111) in terms of Fraunhofer diffraction interferences, using a model of a hard hemisphere on a flat, hard surface. The Fraunhofer diffraction intensities given by this model are[12]

$$P(\theta) \propto \left| \frac{(1+\cos\theta) J_1(kd \sin\theta)}{\sin\theta} \right|^2 , \tag{13}$$

where θ is the scattering angle, d the hard-sphere radius, k the collision wave number, and J_1 denotes the Bessel function of first order. We estimated d from the profile of the equipotential at the collision energy used in the calculation. The effective radius of the adsorbate so defined is $d = 7.5$ bohr. The maximal positions predicted by Eq. (13) are in very good accord with the peaks at $\Delta K_x = \pm 0.48$; ± 0.85; $\pm 1.22\ \text{bohr}^{-1}$ of the exact calculations. Although we view this as sufficient evidence for attributing these peaks to Fraunhofer diffraction, it should be stressed that *the intensities given by the Fraunhofer model (13) are in poor agreement with those of exact calculation:* The intensity ratio of the second-order ($\Delta K_x = 0.85\ \text{bohr}^{-1}$) to the first-order ($\Delta K_x = 0.48\ \text{bohr}^{-1}$) Fraunhofer maximum by Eq. (13) is 0.355, while the exact calculation gives 0.619. (The intensity ratio of the third-order to the first-order maximum gives a much better agreement: 0.184 in Fraunhofer model vs 0.190 of the exact calculation.) This leaves still the maxima at about $\Delta K_x = \pm 2.26\ \text{bohr}^{-1}$ to be physically interpreted. To this effect, and to confirm the interpretations of previous-

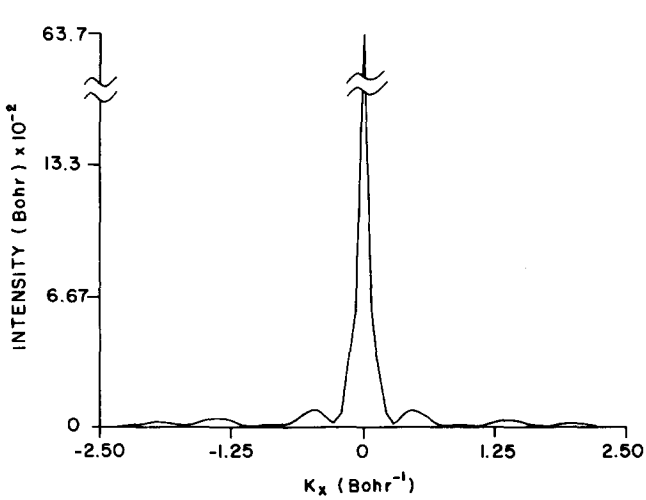

FIG. 1. Angular intensity distribution in He scattering from CO on Pt: Sudden calculations. The results shown are for normal incidence collisions at $k_z = 2.47\ \text{bohr}^{-1}$. The potential used is that of Jonsson *et al.* (Ref. 9).

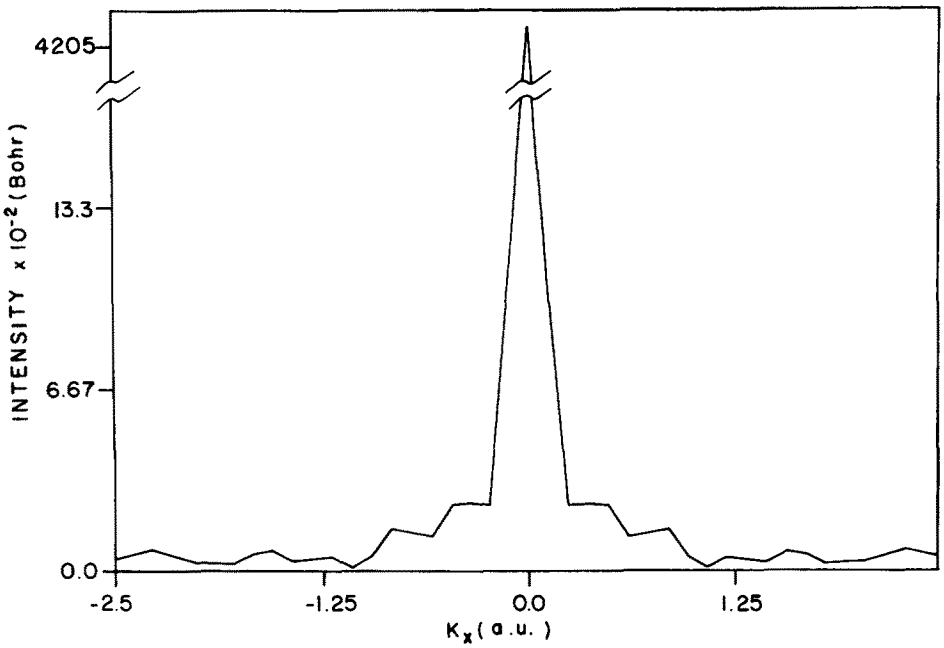

FIG. 2. Angular intensity distribution in He scattering from CO on Pt: Exact quantum calculations. The results shown are for normal incidence collisions at $k_z = 2.47\ \text{bohr}^{-1}$. The potential used is that of Jonsson *et al.* (Ref. 9).

ly mentioned features, we consider the results of classical trajectory calculations for this system. Figure 3 shows the classical intensity distribution for the same collision energy and incidence direction as used above. The maxima seen at $\Delta K_x = \pm 1.20\ \text{bohr}^{-1}$, $\Delta K_x = \pm 2.40\ \text{bohr}^{-1}$ are rainbows. (Although their qualitative shapes are typical of classical rainbows, the spikes are not pronounced due to very limited trajectory statistics in the calculation). A trajectory associated with the rainbow at $\Delta K_x = 1.20\ \text{bohr}^{-1}$ is shown in Fig. 4. The rainbow behavior is due to the fact that this trajectory (and other trajectories at its infinitesimal vicinity) strike the inflection point of the equipotential, which is essentially the same as the inflection point of the phase shift, given by Eq. (11). The inflection point shown in Fig. 4 is due to the corrugation induced by the long-range attractive part of the He/CO interaction at the vicinity of the surface. We expect such inflection points (and the resulting rainbows) to be widely present for adsorbates on flat surfaces, regardless of the quantitative details of the potentials. The rainbows at $\Delta K_x = \pm 1.20\ \text{bohr}^{-1}$ are near in position to the rainbows found in the sudden approximation, Fig. 1, ($\Delta K_x = \pm 1.26\ \text{bohr}^{-1}$), and they are physically of the same origin. The trajectories associated with the classical rainbows at $\Delta K_x = \pm 2.4\ \text{bohr}^{-1}$ are of a different type, shown in Fig. 5: *These are double-collision rainbows, in which the trajectory first strikes the* CO *adsorbate at an inflection point of the equipotential, then undergoes a second collision with the flat Pt surface.* The sudden approximation cannot describe such rainbows, because it does not include double-collision effects. But the peaks corresponding to these rainbows are seen in the exact quantum results of Fig. 2 (at $\Delta K_x = \pm 2.26$

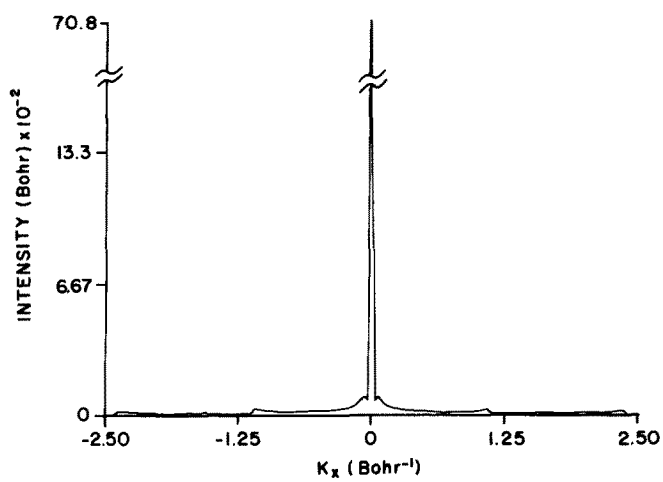

FIG. 3. Angular intensity distribution in He scattering from CO on Pt: Classical trajectory calculations. The scattering conditions and potential are the same as in Figs. (1) and (2).

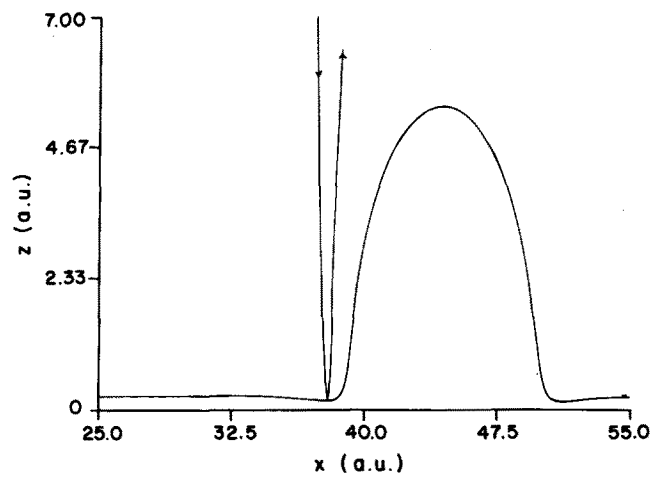

FIG. 4. Trajectory corresponding to single-collision rainbow. The system and scattering conditions are as in Fig. 1. z is the distance from the surface plane and x the coordinate along the 1D surface used. Shown also is the equipotential at the collision energy used. The He atom hits an inflection point of the equipotential.

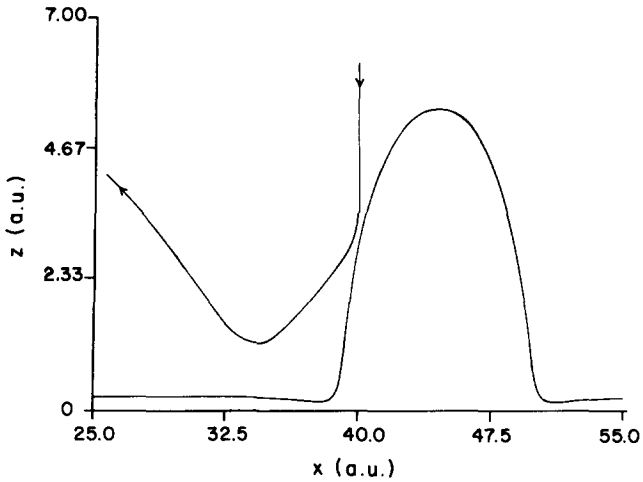

FIG. 5. Trajectory corresponding to double-collision rainbow. The system and scattering conditions are as in Fig. 1. z,x are defined as in Fig. 4. Shown also is the equipotential at the collision energy used. Note that the turning point of the trajectory along z in the second "collision" does not lie on the equipotential, since after the first collision part of the kinetic energy of the atom is in the x direction.

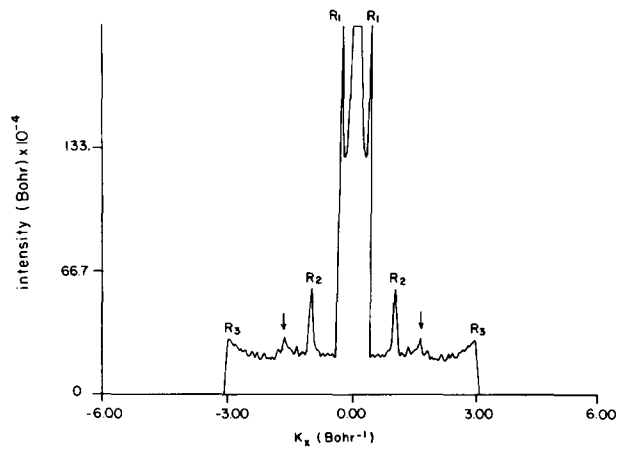

FIG. 7. Intensity distribution from classical trajectory calculations. The energy and incidence direction are as in Fig. 6. R1 is the single-collision rainbow; R2 is the double-collision rainbow corresponding to the trajectory of Fig. 8; R3 is the double-collision rainbow of Fig. 5. The arrows show maxima due to trapping effects.

bohr^{-1}). We sum up now briefly the main findings of this part: (i) Generally, Fraunhofer maxima, single, and double collision rainbow peaks can all be seen in scattering from adsorbates in the same collision conditions (same experiment). (ii) The Fraunhofer maxima are nearer to the specular direction (involve less momentum transfer in parallel to the surface) than either of the rainbows. (iii) The double-collision rainbow occurs at directions much further from the specular than the single-collision rainbow. (iv) The sudden approximation can be used to assign the single collision rainbow, and (at least) the first-order Fraunhofer peak, but not the double collision rainbow. Classical trajectory calculations describe qualitatively both rainbows, but of course cannot yield diffraction interferences. Finally, we note that each of the scattering features discussed here is sensitive to different aspects of the interaction potential. The Fraunhofer maxima mainly probe the size of the adsorbate. The single-collision rainbow probes mainly the long-range force exerted by the adsorbate at the surface plane. The double-collision rainbow is expected to be mostly sensitive to the repulsive He/adsorbate interaction. Experiments measuring all these features should provide a comprehensive picture of the adsorbate/He interaction.

We proceed now to examine the dependence of the Fraunhofer and rainbow effects on the scattering conditions.

B. Dependence of intensity features on incidence energy

We consider now results for He scattering from CO on Pt at normal incidence, but for a collision wave number of $k_z = 3.28$ bohr^{-1}, corresponding to a much higher energy than in the case of Figs. 1–3. Figure 6 shows the exact quantum-mechanical intensity distribution, calculated for the potential of Jonsson *et al.*[9] Figure 7 shows the corresponding classical results. The peaks at $\Delta K_x = \pm 0.52$ bohr^{-1} and

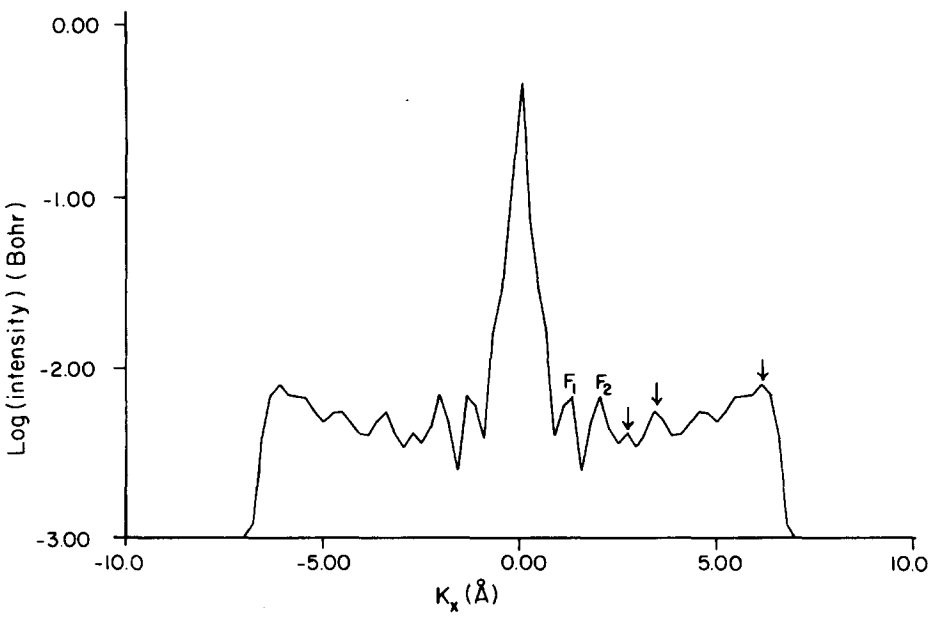

FIG. 6. Angular intensity distribution from exact quantum calculations for He/[CO + Pt]. The results shown are for normal incidence collisions at $k_z = 3.28$ bohr^{-1}. The potential of Jonsson *et al.* (Ref. 9) was used. F1, F2 indicate Fraunhofer peaks. The other maxima are rainbows. Arrows indicate peak positions in the experiments of Lahee *et al.* (Ref. 12).

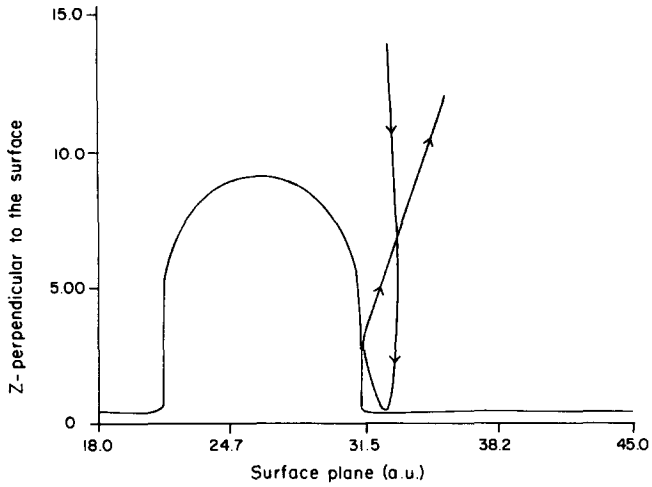

FIG. 8. Trajectory showing the double-collision rainbow R2. The equipotential, corresponding to the collision energy used is also shown.

$\Delta K_x = \pm 1.04$ bohr^{-1} in the quantum intensity distribution seem to be the first- and the second-order Fraunhofer interference maxima: Their positions and magnitudes are in accord with Eq. (13), and they are not present in the classical distributions. The peaks at $\Delta K_x = \pm 1.38; \pm 1.72; \pm 3.05$ bohr^{-1} are all rainbows. It is convenient to classify them with the help of the classical distribution, Fig. 7, and of the trajectories associated with the various peaks. According to this the peaks at ± 1.38 bohr^{-1} are single collision rainbows, of the type shown in Fig. 4, to which we shall refer as R1 rainbows. The peaks at ± 3.05 bohr^{-1} are double collision rainbows, qualitatively the same as in Fig. 5, to which we shall refer as R3. The peaks at $\Delta K_x = 1.72$ bohr^{-1} are a new type of double collision rainbow: The He strike the inflection point on the potential which is due to the long-range attractive part of the He/CO force, but on its way out strikes the CO. The trajectory is shown in Fig. 8, and we refer to this rainbow as R2. Finally, the peaks at $\Delta K_z = \pm 2.75$ bohr^{-1}, $\Delta K_x = \pm 4.3$ bohr^{-1} are to our interpretation supernumerary rainbow peaks of the double-collision rainbow R3. Comparing the angular intensity distribution of Fig. 6 with the lower energy results of Fig. 2, two important facts emerge: First, *at higher energy a new, additional double-collision rainbow emerges.* It clearly requires higher incident momentum than the R3 rainbow mechanism. Second, at *higher energy there are less noticeable Fraunhofer peaks, and more rainbow maxima* (due to the supernumerary peaks). The results of Fig. 6 are in the energy range of the Lahee *et al.*[12] experiments. It may be instructive to make a tentative, limited comparison between the theoretical and the experimental results, for which purpose we show also results of wave packet calculations at $k_z = 5.13$ bohr^{-1} (in Fig. 9), which also correspond to an experimental energy. We caution that a rigorous comparison between experiment and other present calculations is not possible because the calculations brought here show the intensities as a function of momentum transfer (or scattering angle) for fixed (normal) incidence, while in the experiments the final and the initial angle were related (e.g., $\theta_i + \theta_f = 90°$), and thus the intensities compared are not identical). It is nevertheless regarded as provoking that the experimental peaks appear to coincide, to good approximation, with peaks found in the calculations both in Figs. 6 and 9. Should this comparison be reliable, then it would suggest that the maxima actually seen in the experiments of Lahee *et al.*[12] were all rainbows. The true Fraunhofer peaks were not observed, and may well be buried under the specular signal.

C. Dependence of rainbows on incidence angle

Figure 10 shows the classical intensity distribution for a collision at incoming energy of 17.5 meV, and incidence angle of 30°. Figure 11 shows results for the same collision energy at incidence angle of 70°. The results exhibit a physically obvious shadowing effect of the adsorbate on the scattering of the atom. At 70°, the forward ($\Delta K_x > 0$) double-collision rainbows have disappeared completely. As for the backward scattering, Figs. 7, 10, and 11 show that as the

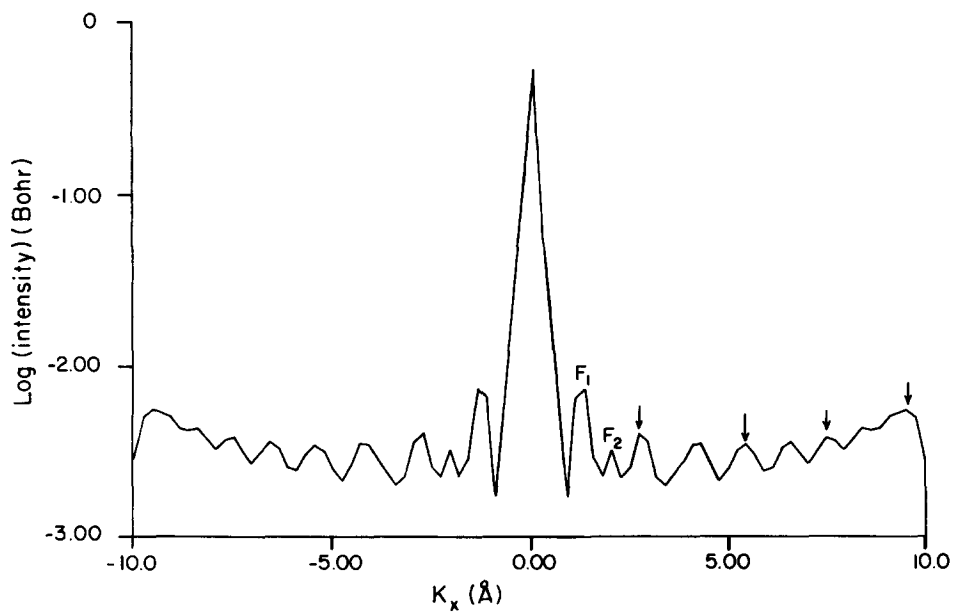

FIG. 9. Angular intensity distribution for He/[CO + Pt] from exact quantum calculations. The results shown are for normal incidence collisions, with $k_z = 5.13$ bohr^{-1}. F1, F2 are Fraunhofer maxima. The other maxima are rainbows. The arrows indicate peak positions in the experiments of Lahee *et al.* (Ref. 12).

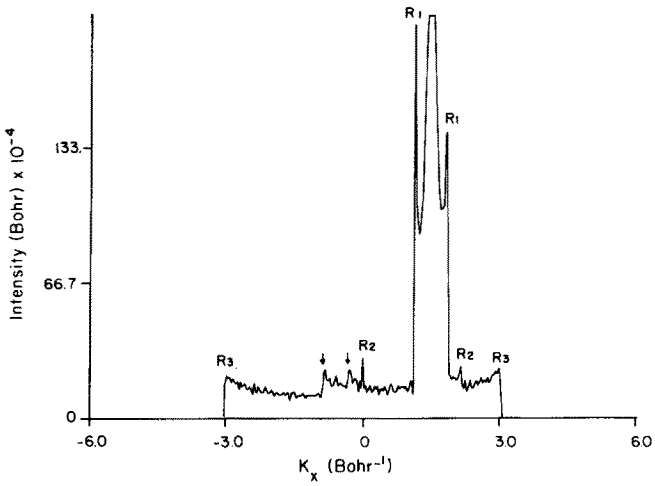

FIG. 10. Classical angular intensity distribution. The results shown are for a collision energy of 17.5 meV, and incidence angle of 30°.

incidence angle is increased also the backward R2 rainbow is suppressed in magnitude in comparison with R1: By geometry one expects at high incidence angles only a small flux of trajectories to hit the inflection point of the potential and then strike the adsorbate, which is required for an R2 rainbow.

D. Dependence of the intensity features on the interaction potential

We examined the sensitivity of the rainbow and Fraunhofer features to the interaction potential. Our calculations have shown that there are only relatively small differences between the results for the Jonsson *et al.*[9] potential, and those obtained using the "gas-phase" interaction, with parameters as given in Sec. II. We focus therefore on the comparison between the angular intensity distribution for the abovementioned potentials and that calculated from the potential of Gumhalter and Liu. Figure 12 shows the scattering intensities calculated using the potential of Ref. 17 for a normal incidence collision with wave number $k_z = 2.5$ bohr^{-1}. The three rainbows R1, R2, and R3 are all seen in the angular intensity distribution although the collision energy is

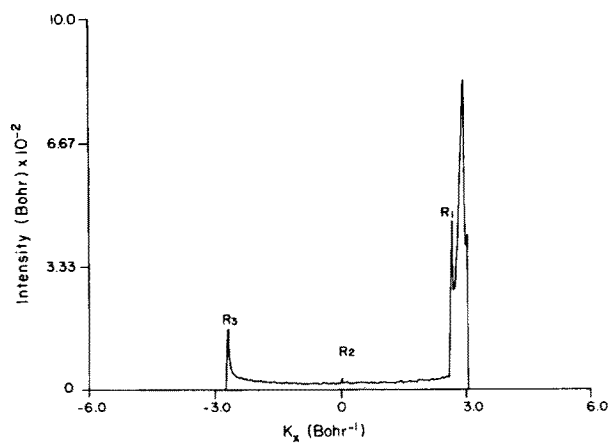

FIG. 11. Classical angular intensity distribution for incidence angle of 70°. The results shown are for a collision energy of 17.5 meV.

low. (The potential of Jonsson *et al.* shows only the R1 and R3 rainbows at such energies.) Analysis of classical trajectory results, not shown here, supports the conclusion on the presence of the third rainbow in this case. The reason for this behavior is that the potential of Liu and Gumhalter, with the parameters used by the authors in Ref. 17 corresponds to a CO molecule placed with its center of mass relatively high above the Pt surface plane. As a consequence, there is an increase in the likelihood of collisions in which the atom hits the repulsive potential of the CO after a previous impact on the Pt surface. The R2 rainbow is caused by collisions of this type. To further reveal the sensitivity of the rainbows to the adsorbate/surface distance, we present now results of a series of calculations in which that distance is varied as a parameter. Fig. 13(a) corresponds to a case in which the CO is almost totally immersed in the conduction electrons of the Pt. The calculations are for a Gumhalter–Liu potential, but with a distance of -1.83 bohr between the CO c.m. and the Pt surface plane. The corrugation due to the CO is slight in this case, and there is hardly any attractive "deformation" of the equipotential away from the adsorbate, as in Fig. 4. Since there is no inflection point in the potential, the R1 rainbow does not appear, and the corrugation is much too low for double-collision rainbows. There is only one pair of peaks seen in Fig. 13(a), and these are first-order Fraunhofer maxima. From Eq. (14) one can extract the effective radius of the CO, R_0, from the peak position. The result obtained is about 4.5 bohr, a small value that indicates that most of the CO is indeed immersed in the Pt for the parameter used, and the corrugation is due to a small part of the CO sphere that lies above the plane of the Pt electrons. The results in Fig. 13(b) correspond to a calculation with the Gumhalter–Liu potential in which the distance of the CO c.m. for the Pt surface is -0.83 bohr. The CO c.m. is such that a significant "attractive" deformation of the equipotential (as in Fig. 4, but much weaker) is already present. Therefore, an R1 rainbow due to scattering from the inflection point, qualitatively as in Fig. 4, does already occur. On the other hand, the repulsive corrugation is still weak, and there is therefore no inflection point on the CO molecule itself, which is required for R3 double-collision rainbows. Also the CO part outside the Pt plane is not high, so collisions that strike the attractive inflection point miss the molecule and will not hit it in a second collision. All this accounts for the fact that in Fig. 13(b) we see Fraunhofer peaks and R1 rainbows, but no R2 or R3 rainbows. Since the CO is less immersed than in the case of Fig. 13(a), the radius of the nonimmersed AP is expected to be higher. From the Fraunhofer model and Fig. 13(b) we estimate $R_0 = 6.25$ bohr, a considerable increase from the previous case. Finally, in the case of Fig. 13(c), the CO c.m. is at a height of $+1.17$ bohr from the Pt surface plane. This corresponds to substantial repulsive corrugation, although still not as with the actual Gumhalter–Liu distance. In Fig. 13(c) the emergence of the R3 (but not yet of R2, as in Fig. 12), rainbow is seen. When measurements of the rainbow features become available, they should, by the above evidence, provide very sensitive information on the adsorbate position with respect to the surface.

We carried out also calculations to check the sensitivity

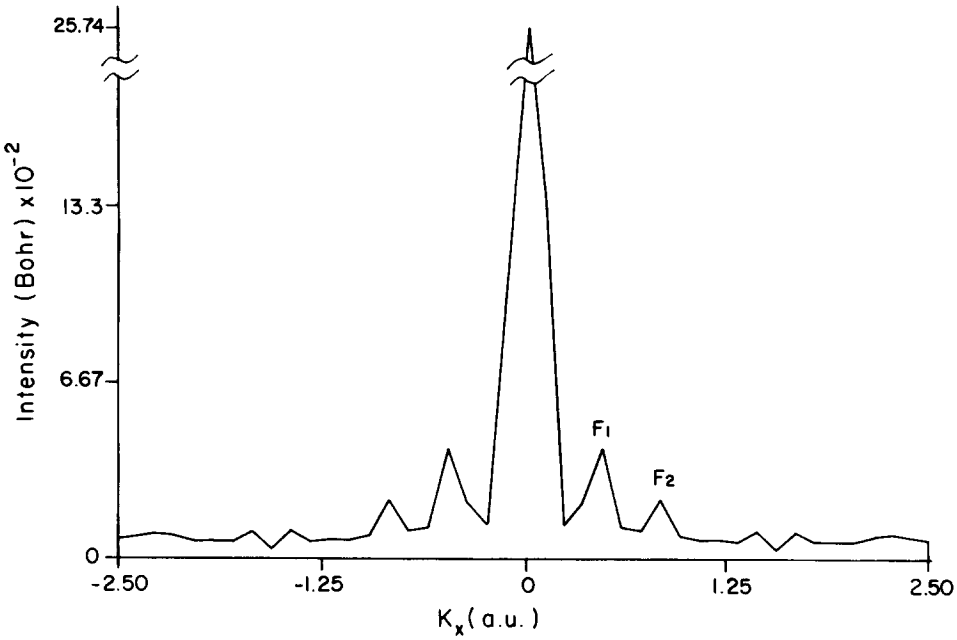

FIG. 12. Angular intensity distribution for the Gumhalter–Liu potential, (exact quantum results). Normal incidence collision, $k_z = 2.5$ bohr^{-1}.

of the rainbow feature, to the surface-mediated interaction terms of the Gumhalter–Liu potential. Although the omission of the image and interference potentials did affect quantitatively the angular intensity distribution, the effects were neither large nor of qualitative interest. This will therefore not be discussed here.

E. Rainbows in scattering from CO on a corrugated surface

We examined this question for a model having much greater corrugation than Pt(111), in order to find significant effects. The potential used in these calculations is described in Sec. II D. Figure 14 shows the results of sudden calculations for He scattering from a CO adsorbate on a corrugated surface. These results show first and second order diffraction peaks due to scattering from the underlying corrugated surface. In addition, there are three symmetrical pairs of rainbows. The identification of these peaks as rainbows is supported by classical trajectory calculations (not shown here), but is mainly based on the fact that these rainbows lie close to values predicted by the stationary-phase approximation, according to Eqs. (11) and (12). These equations, for the potential function of Sec. II D predict rainbows at $\Delta K_x = \pm 0.86, \pm 1.4$, and ± 1.70 bohr^{-1}. The peaks at ± 0.6 bohr are Fraunhofer maxima. All these rainbows are closely related to the attractive inflection point of Fig. 4 in the flat-surface case. However, in the present case the inflection points of the potential (or more precisely the phase shift) involve an interplay between (i) The corrugation induced by the long-range attractive force of the CO molecule at the surface plane; (ii) The corrugation of the surface potential itself. Two of the rainbow pairs are caused by inflection points within the first unit cell adjacent to the CO: one point is closer to the CO molecule, the other is near to an inflection point of the pure surface potential (but amplified and shifted by the CO attractive field). The third rainbow comes from an inflection point in a unit cell one removed from the CO site, but the potential exerted by the CO at this point is still important. The Sudden, of course, only gives single collision rainbows. The classical calculations, which we do not show, exhibit also a double-collision rainbow of the R3 type. Multiple (but single collision) rainbow peaks as in Fig. 14 provide information that should be useful in determining the position of the adsorbate within the surface unit cell, since the latter affects sensitively the inflection points.

F. Adsorbate-induced trapping effects

It is well known that in atom scattering from periodic surfaces of sufficient corrugation there occur resonances that correspond to temporary trapping of the colliding atom in the vicinity of the surface plane. These are referred to as selective adsorption resonances[19] and the study of these resonances has been a major topic in He scattering from crystalline surfaces. Physically, these resonances are due to transfer of energy from the z direction to a direction parallel to the surface plane, caused by the surface corrugation. When the remaining energy in the z direction does not suffice to overcome the binding potential along z, trapping occurs until energy flows back from the (x,y) coordinates of the atom to the direction perpendicular to the surface. For very weakly corrugated surfaces, trapping does not occur or is an extremely weak effect. The question arises whether the local corrugation due to an adsorbate can lead to a trapping effect when the underlying surface is practically flat. This was found to be the case in all the classical low energy calculations that were carried out in this study. We return, for instance, to Fig. 3 showing results for normal incidence impact of He on [CO + (flat) Pt], $k_z = 2.47$ bohr^{-1} (these calculations used the potential of Jonsson *et al.*). Two symmetrical peaks could not be attributed to any rainbow effect. To interpret these peaks, we note first that calculations in this study employed a surface segment on which the adsorbates were placed, and imposed periodic boundary conditions at the ends of the segment. Thus the model used is essentially

one of a lattice of adsorbates upon a flat support, although the distance between the adsorbates in our case was very large. Figure 15 shows trajectories that occur for such a lattice of adsorbates, and the analysis of which has shown it to be the cause of the maxima near the specular: The trajectory strikes a point of inflection on the repulsive wall of the adsorbate, and after the collision is directed towards the flat underlying surface. The energy of the atom in the z direction after the collision with the CO is insufficient for escaping from the surface. The He thus carries out a vibrational motion along z while translating along the surface. It exits from

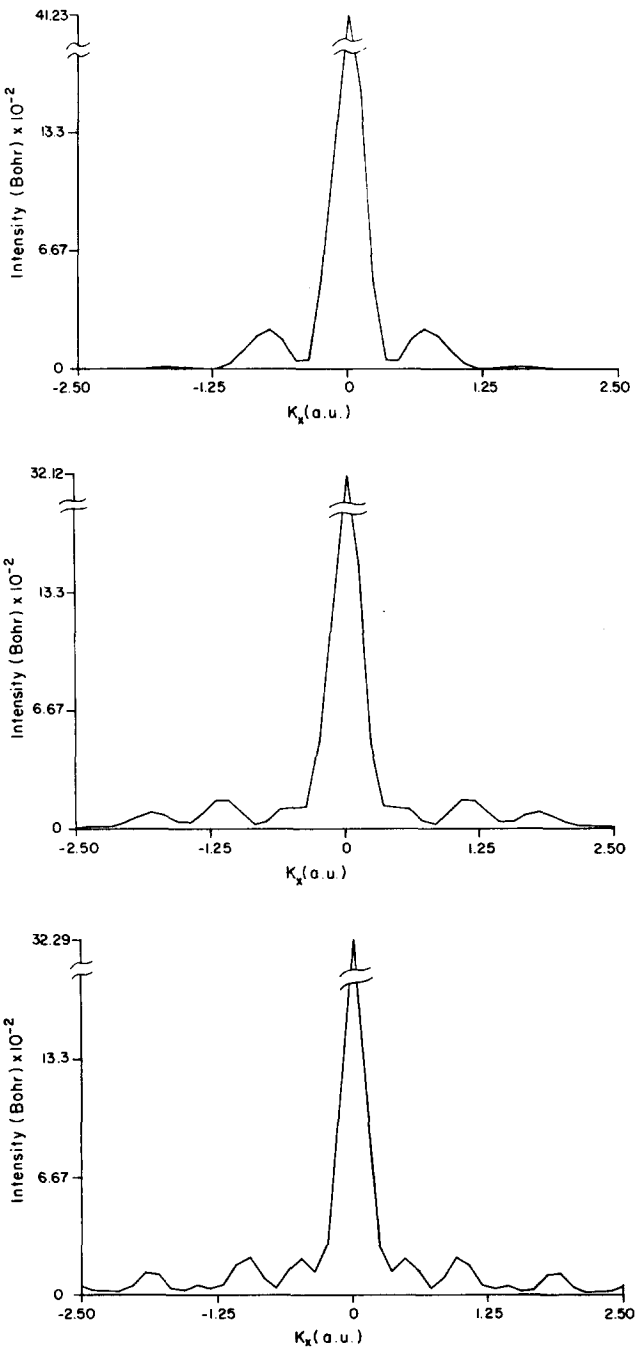

FIG. 13. (a) Angular distribution for the Gumhalter–Liu potential, with an unrealistic distance of CO to surface plane. The CO c.m. is -1.83 bohr, corresponding to immersion of nearly all the molecule in the Pt; (b) As in Fig. 13(a), but with CO c.m. distance to the Pt plane of -0.83 bohr; (c) As in (a), but with CO c.m. distance to the Pt plane of $+1.17$ bohr.

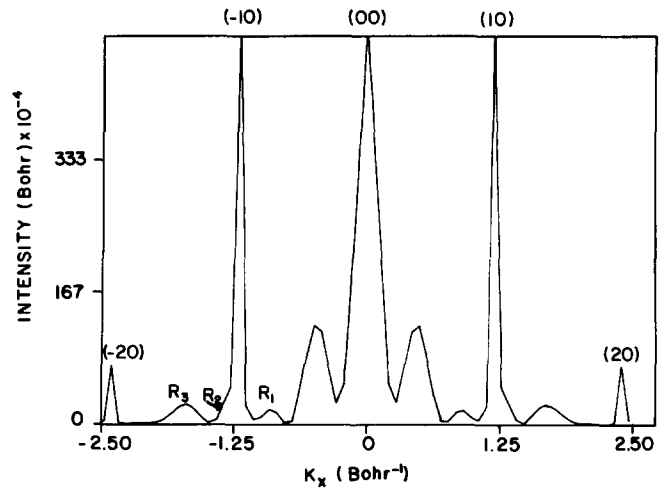

FIG. 14. Angular intensity distribution of He scattered from CO on a corrugated surface. The results are from sudden calculations and correspond to normal incidence collisions at $k_z = 2.47$ bohr^{-1}.

the surface when a collision with a second adsorbate (present in the calculation by virtue of the periodic boundary condition) converts back most of the x-coordinate energy into kinetic energy along z. *The effect appears to be pronounced only when the He actually strikes an inflection point on the equipotential: It can therefore be described as rainbow-enhanced trapping.* The peaks associated with rainbow-enhanced trapping are also seen clearly in Fig. 7, at a somewhat higher energy. It is hard to identify the trapping peaks of Fig. 3 in the quantum angular intensity of Fig. 2, because they are masked by the stronger Fraunhofer effect at the pertinent angles. To pursue the occurrence of the trapping effects quantum mechanically, it is most useful to employ the probability density current, defined in Eq. (7) as a tool of interpretation. Figures 16(a)–16(e) show the probability density current (z,x,t) obtained from the time-dependent wave packet calculations at different points t in time. The results are for normal incidence collisions at $k_z = 3.28$ bohr^{-1}, and

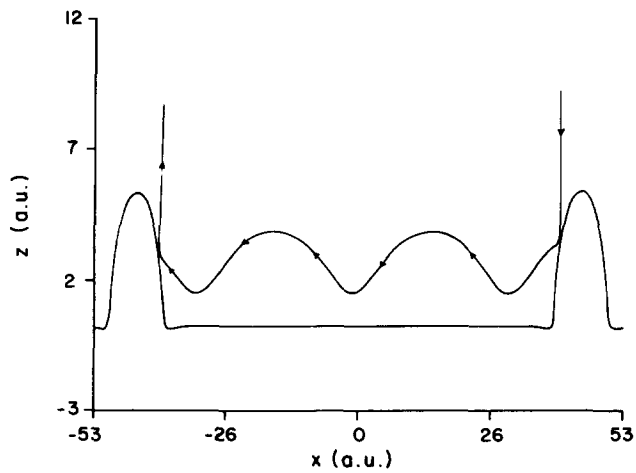

FIG. 15. Trajectory corresponding to rainbow-enhanced trapping in He scattering from [CO on flat Pt]. The potential and scattering conditions are as in Fig. 3. The peaks due to the above (and neighboring) trajectories are seen at the sites of the specular peak in Fig. 3.

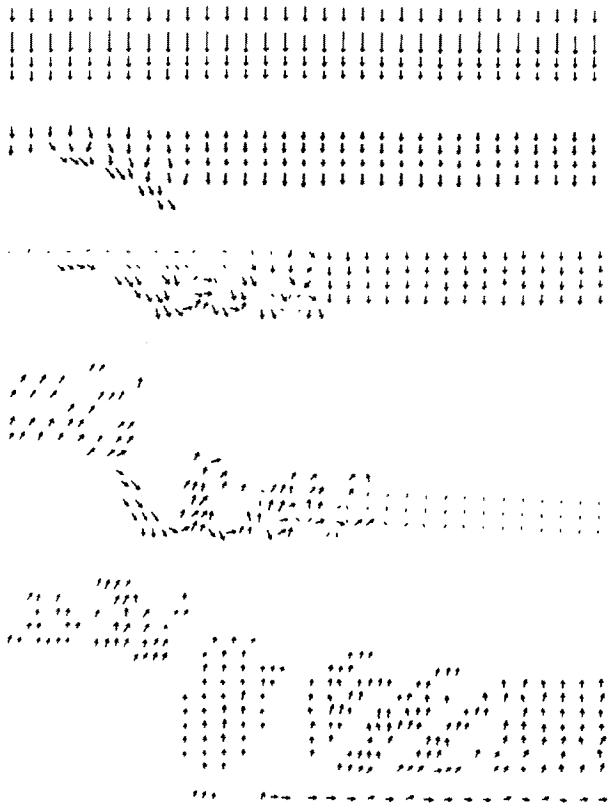

FIG. 16. (a) Contours of the probability density current for He scattering from CO on Pt. The results are for normal incidence collisions at $k_z = 3.28$ bohr^{-1}. The wave packet calculations used the potential of Jonsson *et al.* The arrows indicate the magnitude and direction of $\mathbf{j}(z,x,t)$. The result is for $t = 1.7019\times10^{-13}$s; (b) As in (a), for $t = 5.0887\times10^{-13}$ s; (c) As in (a), for $t = 8.4756\times10^{-13}$ s; (d) As in (a), for $t = 1.1862\times10^{-12}$ s; (e) As in (a), for $t = 1.5249\times10^{-12}$s.

the potential of Jonsson *et al.* was used. Each figure shows the contours of the probability current $|\mathbf{j}(z,x,t)|$ at a given time t. The arrows show the direction of the vector $\mathbf{j}$ at the (z,x) point. Figure 16(a) shows the situation before the wave packet hits the adsorbate. Figure 16(b) shows the onset of wave motion around the repulsive CO sphere, as the wave front reaches the repulsive wall. This motion around the sphere gives rise to some turbulent flow of the probability density, which, as shown in Fig. 16(c), leads to the build up of a Fraunhofer interference peak. Other peaks which include interference contributions build up as the wave front is reflected away from the surface, and the currents associated with the rainbow peaks are clearly visible in Fig. 16(d). There is, however, a component of the wave that leaves the scattering region considerably later than the first front of the probability current. This time-delayed part is clearly the trapped component in Fig. 16(e). We conclude that the quantum calculations do exhibit trapping resonances in analogy with the classical situation. The complexity of the quantum intensity pattern makes it easier to reveal the resonances in terms of an analysis in time, but they also affect the intensities. This, in itself, does not, of course, provide a useful guide on how these (rainbow enhanced) trapping resonances can be measured. A promising approach, in our opinion, will involve a study of a rainbow or a diffraction peak intensity as a function of incidence angle, a sharp reduction in the rainbow (or Fraunhofer) flux being a signature of formation of a trapped component. This is in analogy to the way of measuring selective adsorption resonances in scattering from corrugated periodic surfaces.[19] This topic will, however, be left to a more extensive study in the future.

V. CONCLUDING REMARKS

In this study we sought to demonstrate that the angular intensity distribution of atoms scattered from isolated adsorbates has a rich structure, and that structure contains very useful information on the interaction between the atom and the adsorbate, as well as on the collision dynamics. We found that rainbows and Fraunhofer diffraction interferences can both be seen in the angular intensity distribution, the rainbows occurring at higher momentum transfer than the Fraunhofer peaks. It was also pointed out that the Fraunhofer maxima, the single and the double collision rainbows are each sensitive to a different aspect of the He/adsorbate interaction. The full angular intensity distribution should thus amount to a fairly detailed picture of the adsorbate and its interaction with the colliding atom. Finally, attention was drawn to the occurrence of scattering resonances induced by the presence of the adsorbate. Such resonances, if found, may become a useful additional probe of isolated adsorbates. This, of course, gives rise to the question on the nature of the bound states for a gas-phase atom at the site of an adsorbate, or another surface defect.

It should be desirable to explore the nature of the scattering intensities also for other types of defects, such as vacancies, and work along these lines is in progress. Above all, progress on this topic depends on advance made in the experiments, and we feel these should be strongly encouraged. Although the effects discussed here are hardly easily detectable, by our estimates most of them should be observable with present-day techniques and resolutions. On this basis one may anticipate considerable advance in knowledge of surface defects and their interaction with incoming atoms.

ACKNOWLEDGMENTS

The authors would like to thank Professor G. Comsa for helpful discussions. This work was supported by Grants No. 8400031 and No. 8400019 from the U.S.–Israel Binational Science Foundation to R. B. G. and R. K., respectively. The Fritz Haber Research Center is supported by the Minerva Gesellschaft für die Forschung, mbH, München, BRD.

[1] B. Poelsema and G. Comsa, Faraday Discuss. Chem. Soc. **80**, 16 (1985).
[2] B. F. Mason, R. Caudano, and B. R. Williams, Phys. Rev. Lett. **47**, 1141 (1981).
[3] B. Poelsema, S. T. de Zwart, and G. Comsa, Phys. Rev. Lett. **49**, 578 (1982); **51**, 522 (1983).
[4] B. Poelsema, L. K. Verheij, and G. Comsa, Phys. Rev. Lett. **49**, 1731 (1982).
[5] B. Poelsema, R. L. Palmer, and G. Comsa, Surf. Sci. **136**, 1 (1984).
[6] J. Jonsson, J. H. Weare, and A. C. Levi, Phys. Rev. B **30**, 2241 (1984).
[7] W.-K. Liu, Faraday Discuss. Chem. Soc. **80**, 17 (1985).
[8] S. Bosanac and M. Sunic, Chem. Phys. Lett. **115**, 75 (1985).
[9] A. T. Yinnon, R. Kosloff, R. B. Gerber, P. Poelsema, and G. Comsa, J. Chem. Phys. (in press).

[10](a) R. B. Gerber, A. T. Yinnon, and R. Kosloff, Chem. Phys. Lett. **105**, 523 (1984); (b) A. T. Yinnon, R. Kosloff, and R. B. Gerber, Chem. Phys. **87**, 441 (1984).
[11]M. Heuer and T. M. Rice, Z. Phys. B **59**, 299 (1985).
[12]A. M. Lahee, J. R. Manson, J. P. Toennies, and Ch. Wöll, J. Chem. Phys. **86**, 7194 (1987).
[13]G. Drolshagen and R. Vollmer, J. Chem. Phys. **87**, 4948 (1987).
[14]R. B. Gerber, Chem. Rev. **87**, 29 (1987).
[15]H. P. Butz, R. Feltgen, H. Pauly, and H. Vehmeyer, Z. Phys. **247**, 70 (1971).
[16]J. Harris, A. Liebsch, G. Mechtersheimer, B. Poelsema, and S. Tomoda, Surf. Sci. **118**, 279 (1982).
[17]W.-K. Liu and B. Gumhalter, International Center for Theoretical Physics, Trieste, Report IC/86/77.
[18]R. G. Gordon and R. P. McGinnis, J. Chem. Phys. **55**, 489 (1971).
[19]F. O. Goodman and H. Y. Wachman, *Dynamics of Gas–Surface Scattering* (Academic, New York, 1976).
[20]D. Kosloff and R. Kosloff, J. Comput. Phys. **52**, 35 (1983); R. Kosloff and D. Kosloff, J. Chem. Phys. **79**, 1823 (1983).
[21]H. Tal-Ezer and R. Kosloff, J. Chem. Phys. **79**, 1823 (1983).
[22]R. B. Gerber, R. Kosloff, and M. Berman, Comput. Phys. Rep. **5**, 61 (1986).
[23]R. B. Gerber, A. T. Yinnon, and J. N. Murrell, Chem. Phys. **31**, 1 (1978).
[24]J. I. Gersten, R. B. Gerber, D. K. Dacol, and H. Rabitz, J. Chem. Phys. **78**, 4277 (1983).
[25]A. T. Yinnon, R. B. Gerber, D. K. Dacol, and H. Rabitz, J. Chem. Phys. **84**, 5955 (1986).
[26]D. K. Dacol, H. Rabitz, and R. B. Gerber, J. Chem. Phys. **86**, 1616 (1987).
[27]A. Messiah, *Quantum Mechanics* (North-Holland, Amsterdam, 1964), Vol. I, p. 121.
[28]G. Drolshagen and E. J. Heller, Surf. Sci. **139**, 260 (1984).